Reacting flows simulation with applications to ground to flight extrapolation

P.F. Barbante
Researcher, Politecnico di Milano, Dept. of Mathematics
P.zza Leonardo da Vinci 32, 20133 Milano, Italy
barbante@mate.polimi.it

Abstract

The development of next generation reusable space vehicles requires a precise qualification of their Thermal Protection System materials. The catalytic properties are usually determined in plasma wind tunnels for sets of test conditions relevant to the planned flight mission program. Therefore, for such a situation, it is important to have a methodology that allows for the correct extrapolation of the ground test conditions to the real flight ones and vice-versa. The Local Heat Transfer Simulation concept presented in this paper is a possible strategy to accomplish such a task. The computational results show that the ground test conditions are indeed correctly extrapolated to the flight ones and a simple method to account for possible discrepancies between the two configurations is presented.

1 Introduction

Design and testing of Thermal Protection System (TPS) materials, that are used to protect space vehicles from heat load during the (re-)entry phase, are a major issue for the definition of space missions [20, 17]. The determination of the catalytic properties of TPS materials is especially crucial for the design of an optimal flight strategy: by a matter of fact the stagnation region heat flux for a fully catalytic wall can be more than twice the heat flux for a noncatalytic one [1]. Such situation requires ground facilities able to provide representative testing conditions for the evaluation of the material performances. It is clear that TPS materials should be tested in real flight conditions, in order to safely rely on their catalytic properties. However it is also well known that the complete real flight conditions cannot be exactly duplicated in a ground test facility [19]. The usual strategy to overcome such a problem is to resort to some kind of partial simulation: only some characteristics of the flight environment, that are of interest in the specific experiment, are reproduced [21].

Plasma wind tunnels that can provide dissociated flows for large characteristic time have been widely exploited, in particular for stagnation point testing configuration. Both supersonic arc-jet wind tunnels [22] and subsonic plasma wind tunnels [16] (also known as Plasmatron facilities) have been demonstrated suitable for TPS catalycity studies. The testing methodology in subsonic plasma flows has also been implemented for the high enthalpy facilities at the von Karman Institute (VKI). This approach of catalycity determination makes use of dedicated experimental procedures, combined with accurate CFD computations of the flowfield inside the ground facility [9, 10, 7].

In this contribution we want to start from experimental test results pertinent to the subsonic test methodology and to extrapolate them to the corresponding real flight application. The results allow to verify the hypothesis of the flight extrapolation methodology and to discuss detailed features of hypersonic flows.

2 Local Heat Transfer Simulation for Stagnation Point

One of the most critical parts of a (re-)entry vehicle is the stagnation point region, which is often subject to the highest heat flux; it is therefore important that the testing conditions in the ground facility correctly

Barbante, P.F. (2007) Reacting Flows Simulation with Applications to Ground to Flight Extrapolation. In *Experiment, Modeling and Simulation of Gas-Surface Interactions for Reactive Flows in Hypersonic Flights* (pp. 14-1 – 14-20). Educational Notes RTO-EN-AVT-142, Paper 14. Neuilly-sur-Seine, France: RTO. Available from: http://www.rto.nato.int/abstracts.asp.

reproduce at least the real flight environment around the stagnation point of the aerospace vehicle. The other way around, one has also to be able to correctly determine to which flight conditions the ground test conditions correspond. When we talk about flight conditions we mean a set of freestream conditions, i.e. pressure, temperature, Mach number, that will reproduce, in the boundary layer near the stagnation point of the space vehicle, the same kind of environment found in the ground facility.

We consider the Fay and Riddell [11] and Goulard [13] formulae for the heat flux at the stagnation point of a body immersed in a reacting flow.

The Fay and Riddell formula reads:

$$q_w = 0.76 Pr^{-0.6} (\rho_e \mu_e)^{0.4} (\rho_w \mu_w)^{0.1} \beta_e^{0.5} (H_e - h_w) \left[1 + (Le^{\alpha} - 1) \frac{h_{D,e}}{H_e} \right] \tag{1}$$

$h_{D,e}$ is the dissociation enthalpy (it is equal to $\sum_{i=1}^{Ns} y_{i,e} \Delta h^0_{F,i}$, $\Delta h^0_{F,i}$ being the enthalpy of formation of species i and $y_{i,e}$ their mass fractions). The exponent α is equal to 0.52 for an equilibrium boundary layer and to 0.63 for a frozen boundary layer with fully catalytic wall. β_e is the velocity gradient at the boundary layer outer edge.

The Goulard formula is valid for a frozen boundary layer with an arbitrarily catalytic wall and it reads:

$$q_w = 0.664 Pr^{-2/3} (\beta_e \rho_e \mu_e)^{0.5} H_e \left[1 + (Le^{2/3} \phi - 1) \frac{h_{D,e} y_e}{H_e} \right] \tag{2}$$

y_e is the atom mass fraction at the boundary layer edge and ϕ is a factor that takes into account the wall catalycity.

These two very similar formulae state that the stagnation point heat flux is a function of velocity gradient, flow enthalpy, density and chemical composition (which appears in the determination of the dissociation enthalpy $h_{D,e}$) at the boundary layer outer edge and of the wall enthalpy and catalycity. The ground simulation is correct when the boundary layer conditions are the same in the wind tunnel and in flight: as a consequence the heat flux is equal in the two cases if the wall conditions and the outer edge enthalpy, chemical composition, density or pressure and velocity gradient are the same for wind tunnel and flight.

Under the somewhat restrictive assumption that the flow is near equilibrium, it follows that the heat flux in the stagnation region is the same in flight and in the wind tunnel if the total enthalpy (H_e), the pressure (p_e) and the velocity gradient (β_e) at the outer edge of the boundary layer are the same:

$$H_e^f = H_e^t \qquad p_e^f = p_e^t \qquad \beta_e^f = \beta_e^t \tag{3}$$

We assume the testing conditions are known and we determine the freestream flight conditions and the flying body geometry that will ensure the needed values of H_e, p_e and β_e in the stagnation region. Such a task is accomplished by means of the formulae:

$$h_\infty^f + \frac{1}{2} {V_\infty^f}^2 = H_e^t \tag{4}$$

$$p_\infty^f + \rho_\infty^f {V_\infty^f}^2 = p_e^t \tag{5}$$

$$\sqrt{\frac{8}{3} \frac{\rho_\infty^f}{\rho_e^f}} \, \frac{V_\infty^f}{R_\infty^f} = \beta_e^t \tag{6}$$

Eqs. (4) and (5) are the conservation of energy and momentum for the monodimensional flow on the stagnation line respectively; Eq. (6) is an expression for the velocity gradient computed from the thin shock layer theory [18] (where R_∞^f is the nose radius of the flying body). Although these equations provide only an approximate description of the phenomena that are really happening on the stagnation line, they are still accurate enough for the determination of the flight conditions, as it will be shown by the results. Eq. (4) can

be simplified by taking into account that, at hypersonic flight speed, $h^f_\infty \ll \frac{1}{2}{V^f_\infty}^2$; similarly Eq. (5) is simplified by means of the inequality $p^f_\infty \ll \rho^f_\infty {V^f_\infty}^2$. With these simplifications Eq. (4) gives the flight speed, Eq. (5) the freestream density and therefore the altitude (for example using the US Standard Atmosphere tables) and Eq. (6) the flying body nose radius, all the other quantities being known.

The Local Heat Transfer concept for stagnation region is validated with two series of computations each one performed for different levels of wall catalycity. Ground facility boundary layer outer edge flow conditions are taken from VKI plasma wind tunnel experiments. The first series of computations characterizes the flowfield at the stagnation point of the TPS sample, the second series of computations defines the corresponding real flight situation.

3 Governing Equations and Numerical Methods

We consider axisymmetric configurations and laminar flow. The fluid is made out of N_S chemical species, each one being a thermally perfect gas. Transport coefficients (viscosity μ, thermal conductivity λ, binary diffusion coefficients $\mathcal{D}_{ij}$) are computed with the Chapman-Enskog method [6]; thermodynamic properties are computed by means of statistical mechanics [6]: in the calculations shown here, the rigid rotator, harmonic oscillator model is chosen for the molecular species. An important point is that diffusion fluxes are computed by means of the exact Stefan-Maxwell equations [2, 23] instead of the simplified and inconsistent Fick's law often found in literature. This choice is necessary if one wants to correctly compute the heat flux [23, 2] and it is therefore mandatory for the correctness of the Local Heat Transfer Simulation technique. The chemical forward reaction rates are computed from Arrhenius data fits given in Ref. [14]; the backward reaction rates are computed from the forward ones and the equilibrium constant; the latter being computed from statistical mechanics [6]. Wall chemical reactions are taken into account by means of a wall catalycity model which allows a correct reproduction of the TPS material properties [4, 2].

As already mentioned, the first series of computations is performed in the stagnation region of the TPS material sample; a boundary layer code developed by the author is used [4]. This choice is justified by the fact that boundary layer equations are perfectly equivalent to Navier-Stokes ones in the stagnation point [24]. Once the Lees-Dorodnitsyn coordinate transformation is applied [4, 2] the boundary layer equations on the stagnation line reads:

Continuity:

$$\frac{\partial \tilde{V}}{\partial \hat{\eta}} + F = 0 \tag{7}$$

Momentum:

$$\tilde{V}\frac{\partial F}{\partial \hat{\eta}} = \frac{1}{2}\left(\frac{\rho_e}{\rho} - F^2\right) + \frac{1}{2}\frac{\rho_e v_e}{\rho {\beta^t_e}^2}\frac{\partial \beta^t_e}{\partial y} + \mathcal{K}^2\frac{\partial}{\partial \hat{\eta}}\left(l_0\frac{\partial F}{\partial \hat{\eta}}\right) \tag{8}$$

Species continuity:

$$\tilde{V}\frac{\partial y_i}{\partial \hat{\eta}} + \mathcal{K}\frac{\partial J_i}{\partial \hat{\eta}} = \dot{w}_i \tag{9}$$

Energy:

$$\tilde{V}\frac{\partial g}{\partial \hat{\eta}} = \mathcal{K}^2\frac{\partial}{\partial \hat{\eta}}\left(\frac{l_0}{Pr}\frac{\partial g}{\partial \hat{\eta}}\right) - \mathcal{K}^2\frac{\partial}{\partial \hat{\eta}}\left(\frac{l_0}{Pr}\sum_{i=1}^{Ns}\frac{\partial y_i}{\partial \hat{\eta}}\frac{h_i}{h_e}\right) - \mathcal{K}\frac{\partial}{\partial \hat{\eta}}\left(\sum_{i=1}^{Ns} J_i\frac{h_i}{h_e}\right) \tag{10}$$

Unlike standard stagnation line boundary layer equations written in Lees-Dorodnitsyn variables [2, 12] two additional terms appear: $\mathcal{K}$ and the second term of the r.h.s. of the momentum equation. In the standard Prandtl boundary layer theory the outer edge quantities are computed by extrapolating the external inviscid solution to the wall. In the ground facility a low Mach, low Reynolds number jet impinges on the TPS material sample and it is therefore more appropriate to match the boundary layer (which should be interpreted as a zoom of the stagnation region) and the external flow at the real boundary layer outer edge. The two

extra terms are due to such a matching procedure; $\mathcal{K}$ accounts for the real boundary layer thickness and the second term on the r.h.s. of the momentum equation accounts for the fact that the quantity $\partial u_e/\partial y$ (computed at the boundary layer outer edge) has to be included in the expression of the boundary layer pressure gradient [2]. The factor $\mathcal{K}$ is constant in the boundary layer and it is computed during the numerical solution [2]. The second term on the r.h.s. of Eq. (8) is given by suitable processing of ground experiments data. The procedure combines experimental results with numerical computations of the flowfield inside the ground facility (interested readers are addressed to Refs. [9] and [10]).

The second series of computations, for the real flight condition, is performed by means of a Navier-Stokes finite volume code for reacting flows (which was also developed by the author [3, 2]). The convective terms are discretized with the Hybrid Upwind Splitting Riemann solver [8]; a MUSCL type reconstruction [15] is applied to achieve second order accuracy: Van Albada's limiter is used in the present work. The transport terms are centrally discretized with second order accuracy.

We want to emphasize that the two codes make use of the same set of physico-chemical models, thus allowing for a coherent and physically consistent comparison between the two series of computations; in Ref. [4] it is shown that they provide results in excellent agreement when applied to the same configuration.

4 Flight Data Determination

The external flowfield conditions in the stagnation region of the TPS material sample are taken from data of existing experiments [10, 9]. The first set of data, hereinafter called case (a), has been obtained from VKI Minitorch (a small scale plasma wind tunnel) experiments [9]. The second set of data, hereinafter called case (b), has been taken from experiments carried out in the VKI Plasmatron facility [5].

The following conditions are selected for case (a) (they have to be understood as conditions at the TPS boundary layer outer edge):

$$H_e^t = 9.8\,\frac{MJ}{Kg} \qquad p_e^t = 10161\,Pa \qquad \beta_e^t = 11670\,s^{-1} \tag{11}$$

Under the assumption of local equilibrium, they correspond to a temperature $T_e^t = 4560\,K$ and to a chemical composition where molecular oxygen is almost fully dissociated and molecular nitrogen is just starting to dissociate.

Extrapolation of these wind tunnel conditions to the real flight ones, by means of the procedure described in Sec. (2), gives:

$$\begin{aligned} V_\infty^f = 4430\,\frac{m}{s} \qquad M_\infty^f = 13.7 \qquad z_\infty^f = 55.78\,km \\ p_\infty^f = 38\,Pa \quad T_\infty^f = 258.6\,K \quad R_\infty^f = 17.72\,cm \end{aligned} \tag{12}$$

(z_∞^f is the altitude, determined from the U.S. 1976 Standard Atmosphere). The computed speed value is within upper 10% of the Space Shuttle speed at the same altitude [1]. For simplicity the shape of the (re-)entry body has been taken to be a sphere with a radius equal to R_∞^f. The predicted body nose radius is too small compared with the one of existing or planned (re-)entry vehicles. In this specific case the small value depends from the diameter ($10\,mm$) of the TPS sample that has been used in the experiments. In practice, more realistic values are obtained by using samples of bigger diameter. In any event, for the purpose of the present discussion, i.e. a demonstration of the validity of the Local Heat Transfer concept, the computed nose radius is acceptable.

A more realistic (re-)entry vehicle nose radius is obtained for case (b), to whom the following conditions apply:

$$H_e^t = 22.8\,\frac{MJ}{Kg} \qquad p_e^t = 12525\,Pa \qquad \beta_e^t = 1502\,s^{-1} \tag{13}$$

Under the assumption of local equilibrium, the boundary layer outer edge temperature is $T_e^t = 6085\,K$, molecular oxygen is fully dissociated and nearly 40% of molecular nitrogen is dissociated. The real flight conditions are:

$$V_\infty^f = 6755\,\frac{m}{s} \qquad M_\infty^f = 21.5 \qquad z_\infty^f = 60.96\,km$$
$$p_\infty^f = 19\,Pa \quad T_\infty^f = 244.4\,K \quad R_\infty^f = 1.79\,m \tag{14}$$

The air mixture considered for both cases is a five component mixture; more precisely, molecular oxygen O_2, molecular nitrogen N_2, nitric oxide NO, atomic oxygen O and atomic nitrogen N are used. Due to the relatively low temperature there is no need to take into account ionized species.

As mentioned before, only some characteristics of the flight environment are reproduced in the ground facility. It seems therefore interesting to check which nondimensional parameters are effectively reproduced. We compare two classical nondimensional parameters, the Reynolds number and the Mach number. As characteristic dimension for the flying body and the TPS sample we take the respective diameters. For case (a) the jet speed in the ground facility is $V_\infty^t = 149\,m/s$ and the probe diameter is $10\,mm$. With these values we have: $Re^f = 49600$, $M^f = 13.7$ for the flight and $Re^t = 62$, $M^t = 0.1$ for the ground facility. For case (b) the ground jet speed is $V_\infty^t = 99\,m/s$ and the probe diameter is $50\,mm$. The Reynolds and Mach numbers are: $Re^f = 424000$, $M^f = 21.5$ for the flight and $Re^t = 123$, $M^t = 0.06$ for the ground. Reynolds and Mach numbers are really different in flight and in the wind tunnel, this means that, in the specific configuration, they are not the key parameters for the duplication of the stagnation point heat flux.

5 Flight Extrapolation Results

For the validation of the local heat transfer concept two series of computations have been performed for each test case. The first series is performed along the stagnation line of the TPS material sample by means of the boundary layer method. The second series, for the real flight condition, has been performed by means of the Navier-Stokes finite volume technique.

Six different levels of wall catalytic activity have been taken into account. The wall reaction set is given by: $N + N \rightarrow N_2$ and $O + O \rightarrow O_2$, i.e. we take into account recombination of atomic nitrogen and of atomic oxygen at the wall and we also assume that the wall has no effect on nitric oxide NO. For simplicity, a single value of the catalytic recombination probability γ has been taken for the two reactions. The six different computations correspond to the following values of γ:

$$\gamma = \left\{0;\ \ 10^{-4};\ \ 10^{-3};\ \ 10^{-2};\ \ 10^{-1};\ \ 1\right\}$$

The wall temperature T_w has been taken uniformly equal to $1000\,K$ both on the TPS sample and on the equivalent (re-)entry geometry.

The boundary layer computations have been performed only in the stagnation point: 100 points in the direction across the boundary layer have been taken for both case (a) and case (b). The Navier-Stokes computations have been performed on the front part of the sphere and only half of it has been considered, because of the symmetry with respect to the stagnation line. The grid has 3600 cells for case (a), 5680 for case (b) and it is suitably refined in the boundary layer and in the proximity of the bow shock in order to improve the computational accuracy.

We discuss now the results for case (a). In Fig. 1 the heat flux, computed for the different values of the catalytic recombination probability, γ is shown (the heat flux value for $\gamma = 0$ is not shown because of the logarithmic scale, but it is practically equal to the one for $\gamma = 10^{-4}$). The difference in heat flux between the Navier-Stokes and the boundary layer computations goes from 3% for the case of noncatalytic wall to 37% for the case of fully catalytic wall. Although the difference in heat flux for fully catalytic wall is high, the difference in the case of noncatalytic or low catalytic ($\gamma < 10^{-3}$) wall (which is the case of interest for aerospace applications) is below 6%, i.e. in the range of the experimental uncertainties [16].

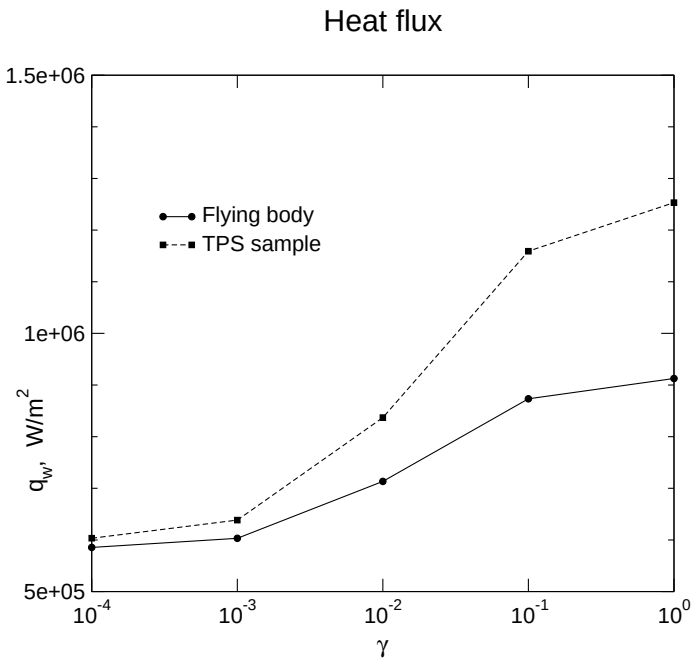

Figure 1: Case (a): stagnation point heat flux for different catalycity levels

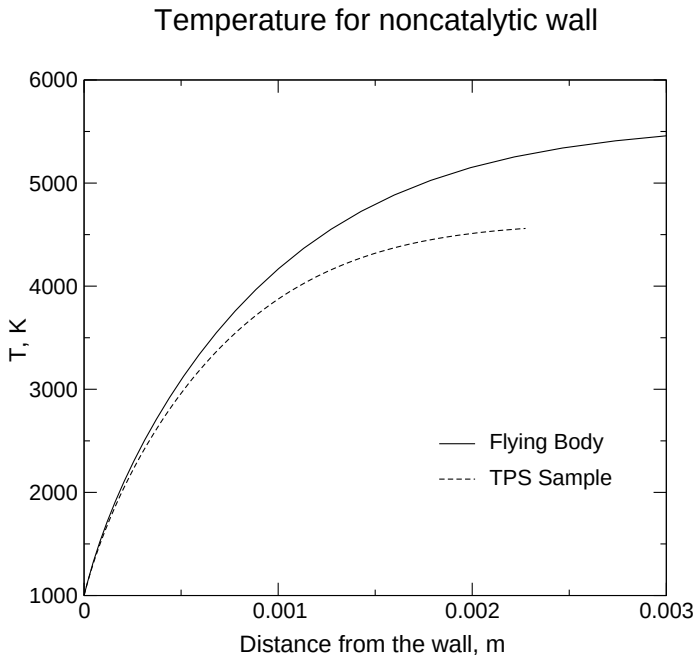

Figure 2: Case (a): temperature profile for noncatalytic wall

The reason for the good agreement between the two computations in the cases of low or noncatalytic wall can be explained by an examination of Figs. 2 and 3. The temperature profiles are similar in the portion of the boundary layer with $y < 0.001\,m$ and the respective slopes at the wall are almost identical (see Fig. 2); this leads to a good agreement on the conductive part ($-\lambda\nabla T$) of the heat flux between the two configurations. Looking at Fig. 3 one can notice that the boundary layer is practically frozen in both computations; the diffusive part of the heat flux ($\sum_{i=1}^{Ns} h_i \vec{J}_i$) is thus negligible in the two cases (and zero for the noncatalytic case). The atomic oxygen mass fraction is higher for the TPS sample than for the

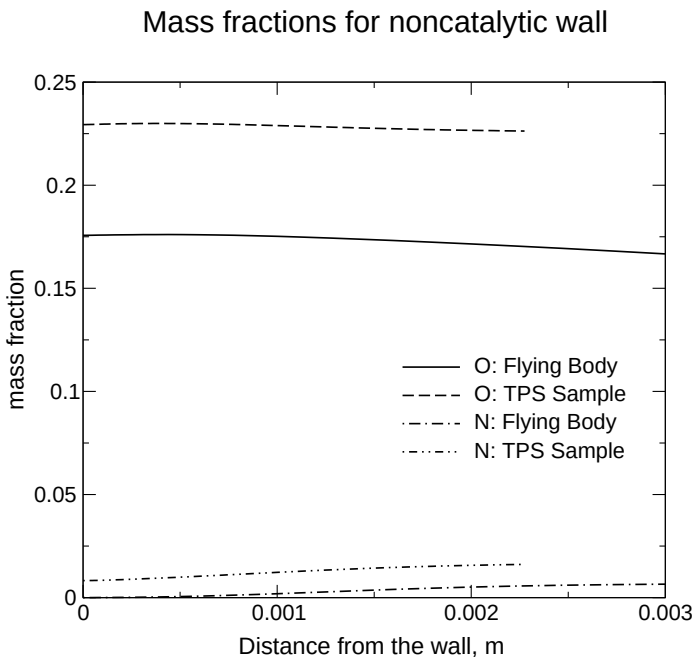

Figure 3: Case (a): O and N mass fractions for noncatalytic wall

flying body, but the two profiles have an almost identical shape, differing only by a constant shift. The same observations are valid for atomic nitrogen. This similar behaviour is not surprising, because Eq. (6) implies the equality of the first Damköhler number in the stagnation region of both TPS sample and real flight body. The inverse of velocity gradient is a time scale of the flow in the stagnation region and it is the same for both configurations; the outer edge temperature and pressure being the same, also the chemical characteristic time is the same and, therefore, the first Damköhler number. Another parameter that has to be correctly reproduced is the second Damköhler number, which characterizes the heterogeneous chemistry-diffusion coupling and therefore the interaction between the TPS material and the reacting gas. The second Damköhler number is defined as: $Da_2 = k_S l^2/D$ where k_s is the inverse of a characteristic time of the wall heterogeneous reactions, D a diffusion coefficient and l a characteristic length over which diffusion takes place (as, for example, the boundary layer thickness). The surface material is the same and, therefore, k_s is the same too; in addition, because pressure, temperature and chemical composition are similar also D is the same. Inspecting Figs. 2 and 3 we notice that the boundary layer thickness l is fairly close in the two configurations: in effect stagnation point boundary layer thickness is a function of the square root of the inverse of velocity gradient [24]. Therefore we deduce that also the second Damköhler number is acceptably duplicated in the ground facility.

Temperature is higher and atomic species mass fractions are lower, at the boundary layer edge in the flying body case than in the TPS sample case, because in the former configuration there is still a certain degree of nonequilibrium in the shock layer, thus violating one of the assumptions on which the Local Heat Transfer Simulation concept is based. However, the influence of the violation is negligible (at least for heat flux determination) in the case of a low catalytic wall. A good reproduction of the behaviour of atomic species, especially oxygen, in the ground facility is important to ensure that phenomena like aging and oxidation of the TPS material are correctly simulated. In the specific case, the overestimation of atomic oxygen mass fraction for the TPS sample in the test configuration gives a certain safety margin.

In Fig. 4 the temperature profiles for fully catalytic wall ($\gamma = 1$) are shown. The agreement is even better than before and the conductive part of the heat flux is within 2% in the two configurations. Therefore, the difference in total heat flux (see Fig. 1) is only due to the diffusive part. From Fig. 5 we notice that atomic species are recombining at the wall because it is fully catalytic. The chemical composition in the boundary

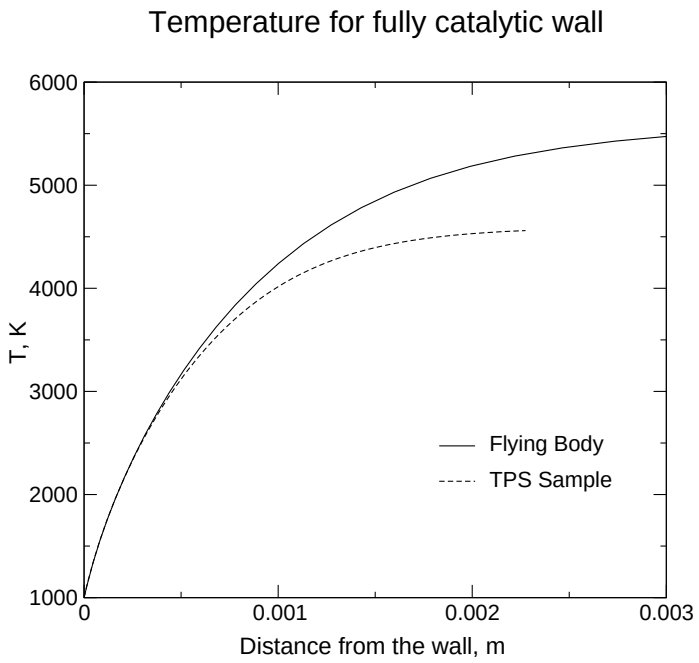

Figure 4: Case (a): temperature profile for fully catalytic wall

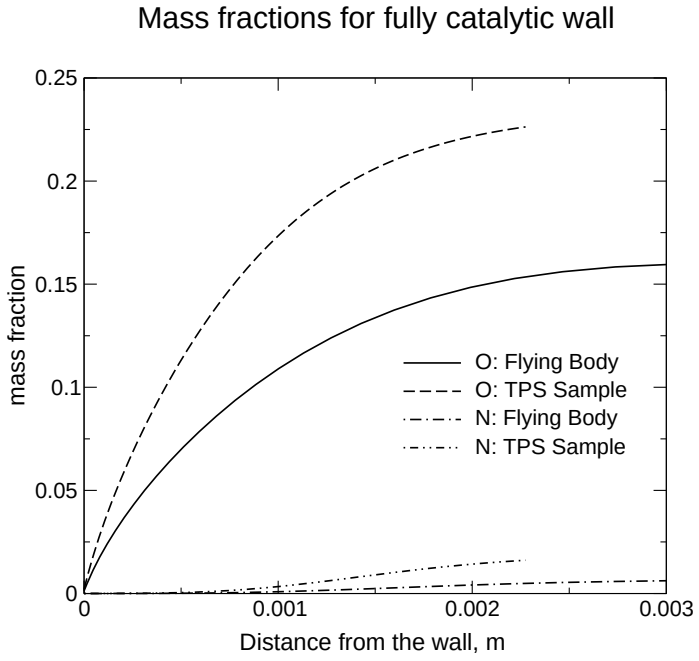

Figure 5: Case (a): O and N mass fractions for fully catalytic wall

layer is dominated in both cases by the wall catalytic reactions $O + O \rightarrow O_2$ and $N + N \rightarrow N_2$. Molecular oxygen and nitrogen created at the wall diffuse toward the interior of the boundary layer, completely changing the picture with respect to the noncatalytic case. We further notice that not only atomic oxygen mass fraction is higher for the TPS sample, but also its slope at the wall. This implies that the diffusive heat flux is higher in the TPS sample case than in the flying body one, thus explaining the observed differences in total heat flux (the contribution of atomic nitrogen recombination to the heat flux is negligible).

Results for case (b) are discussed now. In Fig. 6 the stagnation point heat flux, computed for several

values of catalytic recombination probability γ, is shown. (As in case (a) the heat flux value for $\gamma = 0$ is not shown because of the logarithmic scale, but it is practically equal to the one for $\gamma = 10^{-4}$). Computed heat flux difference between Navier-Stokes and boundary layer goes from 2% for noncatalytic wall to 3% for fully catalytic wall. We notice also that for noncatalytic wall heat flux is higher for boundary layer computations, whilst for fully catalytic wall heat flux is higher for Navier-Stokes computations.

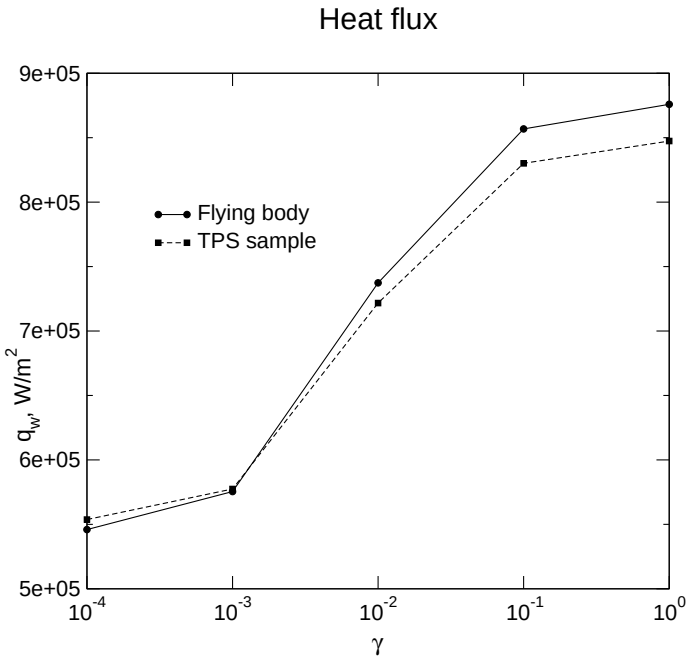

Figure 6: Case (b): stagnation point heat flux for different catalycity levels

In Fig. 7 temperature profiles for noncatalytic wall are shown; the agreement is excellent, in particular close to the wall.

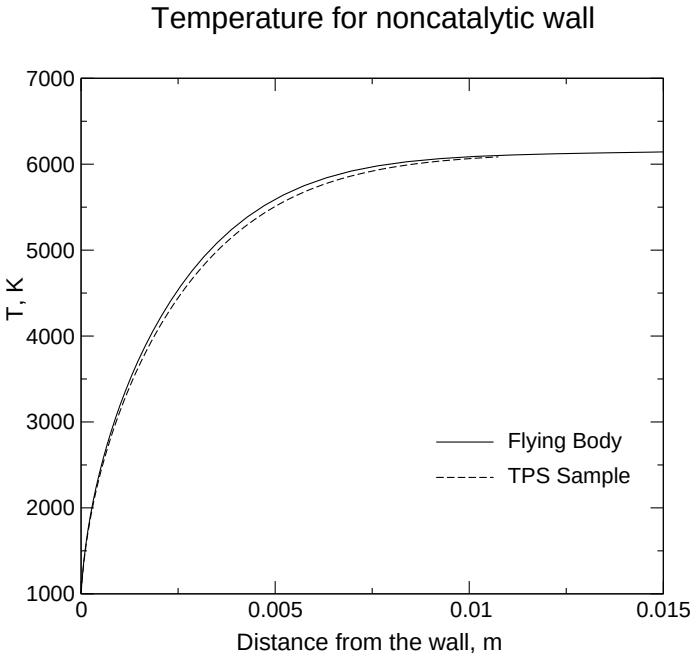

Figure 7: Case (b): temperature profile for noncatalytic wall

In Fig. 8 atomic species profiles for noncatalytic wall are shown. Oxygen is fully dissociated at the boundary layer outer edge and remains fully dissociated all along the boundary layer; agreement between ground and flight profiles is excellent. Nitrogen is partially dissociated at boundary layer edge, the agreement between TPS sample and flying body profiles is good, suggesting that the same physico-chemical phenomena are happening in the two boundary layers. Compared with case (a) we notice a much improved agreement in atomic species profiles. The main reason is the close matching of boundary layer outer edge chemical composition between ground and flight. Chemistry is assumed to be in equilibrium at the TPS boundary layer outer edge and for case (b) is close to equilibrium for flight too: the main reason is the fact that velocity gradient, which is the inverse of the typical flow time in the stagnation region, is now six times smaller than in case (a). We would also like to point out that, as in case (a), boundary layer thickness and first and second Damköhler numbers are well matched for TPS sample and flying body.

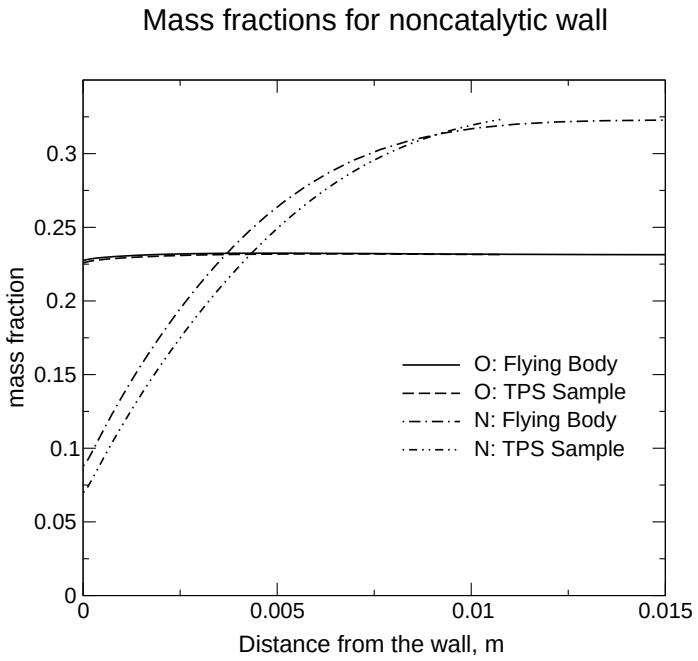

Figure 8: Case (b): O and N mass fractions for noncatalytic wall

In Fig. 9 the temperature profiles for fully catalytic wall are shown. The two temperature profiles are again very close to each other. One can notice that, at the same distance from the wall, temperature is higher for fully catalytic wall than for noncatalytic one.

Atomic species profiles are shown in Fig. 10. Atomic oxygen profile is strongly affected by wall catalytic recombination, because oxygen molecules created at the wall diffuse toward the interior of boundary layer. Atomic nitrogen appreciably recombines in the bulk of boundary layer and its slope at the wall is considerably shallow, although the wall is fully catalytic. Both phenomena, wall dominated recombination for O and gas phase dominated recombination for N, are reproduced with good agreement between TPS sample and flying body. The slope of atomic species profile at the wall is modestly larger in the real body boundary layer, explaining the slightly higher flight heat flux.

From the previous discussion one could conclude that the Local Heat Transfer Simulation concept has only a limited range of validity, i.e. when the conditions at the boundary layer outer edge are close to local equilibrium. However both curves in Fig. 1 and in Fig. 6 are similar and show a strong dependence of the heat flux from wall catalycity in the interval $[10^{-3} - 10^{-1}]$; this suggests that the same physico-chemical trends are reproduced in the ground facility and in flight. In addition, by looking at Fig. 11, we notice that

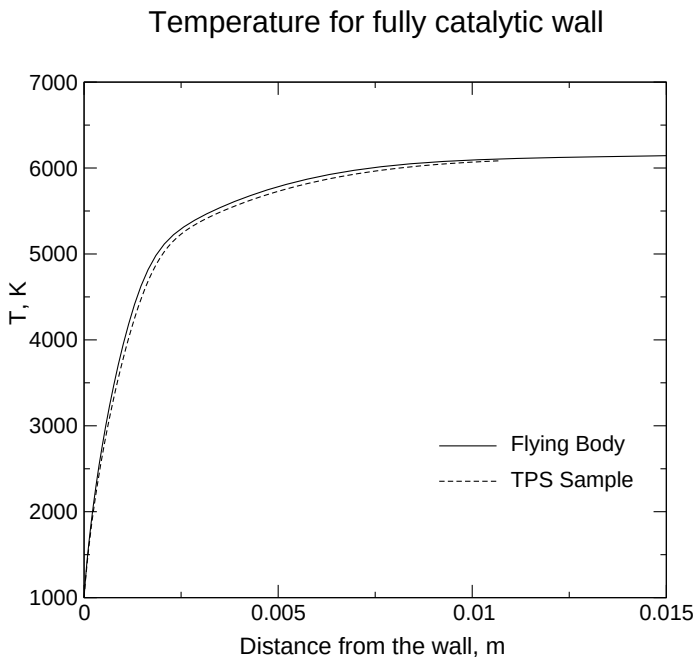

Figure 9: Case (b): temperature profile for fully catalytic wall

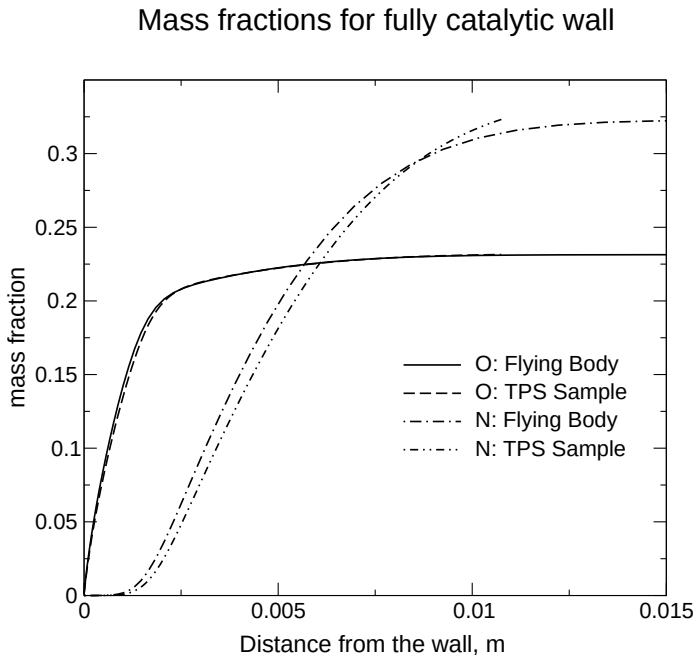

Figure 10: Case (b): O and N mass fractions for fully catalytic wall

the normalized heat flux

$$Q = \frac{q_w - q_w^{NC}}{q_w^{FC} - q_w^{NC}} \tag{15}$$

is very similar for ground and flight in both cases (a) and (b). The excellent agreement between normalized heat fluxes is mainly due to the equality of Damköhler numbers for TPS sample and flying body. The flight

heat flux for an arbitrary value of wall catalycity could therefore be deduced by means of the formula:

$$q_w^f = Q^t \cdot \left(q_w^{f,FC} - q_w^{f,NC} \right) + q_w^{f,NC} \tag{16}$$

where Q^t is computed by means of Eq. (15) with the heat flux values obtained for the TPS sample; these values can also be experimentally measured ones. Eq. (16) is very accurate. Consider, for example, the heat flux value for case (a) with $\gamma = 10^{-1}$: the TPS sample computation overpredicts the heat flux by 22% with respect to the real flight one. If, on the opposite, Eq. (16) is used, the heat flux is underpredicted only by 1%, a really dramatic improvement.

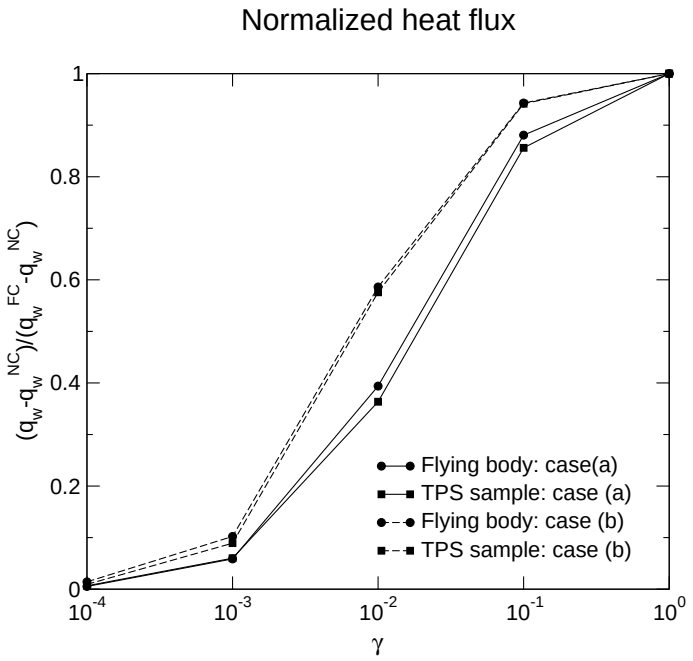

Figure 11: Stagnation point normalized heat flux for different catalycity levels

The normalized heat fluxes presented above (Fig. 11) could be interpreted as the effect of boundary layer chemical activity on the heat transfer. Since the heat flux is always increasing with the wall catalycity the curves will be strictly monotonous. However a curve standing in the lower part of the graph indicates a lower gas chemical activity, while a curve lying in the upper part reveals a higher chemical activity inside the boundary layer. In effect, in the limit case of chemical equilibrium, the heat flux is the same for every possible value of wall catalycity [11] and the normalized heat flux curve collapses into a straight line corresponding to $Q = 1$. The relative position of the curves for case (a) and (b) could therefore be interpreted based on these considerations. Case (a), for instance, denotes a situation where the gas phase chemical activity is lower. This fact is due to the much higher velocity gradient for this case, which promotes a frozen flow at the stagnation region by imposing a lower Damköhler number. This characteristic can be noticed in Fig. 11: the curve for the case (a) appears below the curve for case (b). In addition the inspection of Figs. 3 and 8 clearly points out that chemical activity in the boundary layer is higher in case (b) than in case (a).

6 Local Heat Transfer Simulation for a Flat Plate

The previous discussion has been on stagnation region flowfield; now we would like to present a preliminary discussion of the Local Heat Transfer concept for a flat plate configuration. The main hypothesis we make is that the outer edge boundary conditions are constant along the flat plate: it amounts practically to impose that the boundary layer is everywhere self similar. Assuming also that the boundary layer is frozen we can write,

by means of an approximate analytical solution of the boundary layer equations, a wall heat flux formula that is quite similar to Eqs. 1 and 2:

$$q_w = 0.332 Pr^{-2/3} \frac{\rho_w \mu_w}{(\rho_e \mu_e)^{0.5}} \left(\frac{u_e}{x}\right)^{0.5} (H_e^{ad} - h_w) \left[1 + (Le^{2/3} - 1) \frac{1}{1+\phi_w} \frac{y_e h_{D,e}}{H_e^{ad} - h_w}\right] \tag{17}$$

Where x is the distance from the flat plate leading edge and H_e^{ad} is the recovery enthalpy defined as: $H_e^{ad} = H_e + r u_e^2/2$. The recovery factor r is mainly a function of the Prandtl number and is equal to zero for $Pr = 1$ and less than zero for $Pr < 1$ (which is the case for air reacting mixtures). The factor ϕ_w takes into account the wall catalycity. The formula states that the flat plate wall heat flux is a function of recovery enthalpy, density, chemical composition at the boundary layer outer edge, of the term u_e/x (that has the dimensions of a velocity gradient) and of the wall enthalpy and catalycity. Therefore the heat flux is equal in flight and in the wind tunnel if the previous quantities are the same in both cases. The equality of recovery enthalpy, density and chemical composition implies the equality of outer edge velocity and also of the flat plate dimensions (because u_e/x has to be the same). It seems that it is possible to have the same heat flux only with perfect duplication of real flight conditions and of body dimensions in the wind tunnel. However, if we can tolerate a discrepancy in the heat flux, it is possible to relax the condition on recovery enthalpy and to impose the equality of static enthalpy. The heat flux would be approximately the same in flight and in the wind tunnel if (the assumption that the boundary layer is close to chemical equilibrium at the outer edge is made):

$$h_e^f = h_e^t \qquad p_e^f = p_e^t \qquad \frac{u_e^f}{x^f} = \frac{u_e^t}{x^t} \tag{18}$$

It is clear that, imposing the equality of static enthalpy and not of recovery enthalpy, we cannot obtain an exact duplication of heat flux as in the stagnation point, but only an approximate one; however it is the only way to avoid a one to one duplication of the flight environment in the wind tunnel.

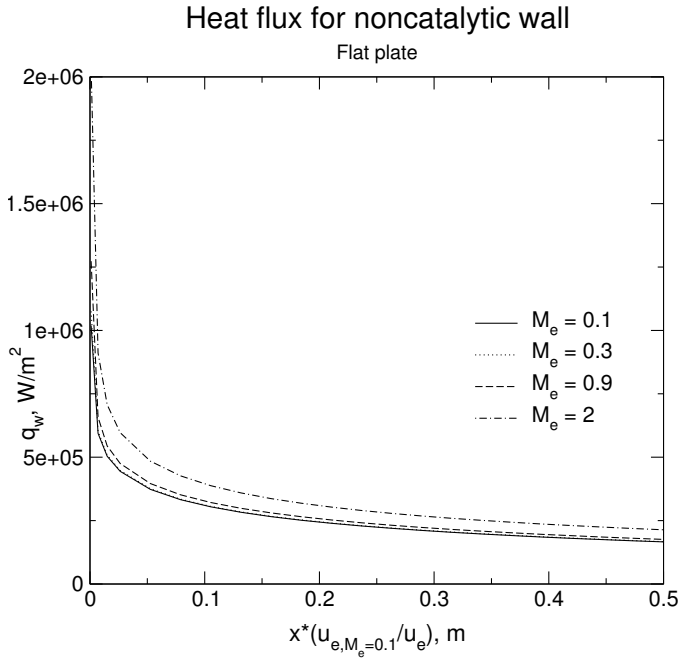

Figure 12: Flat plate heat flux for noncatalytic wall

We present now a few computations that are meant to provide a preliminary assessment of the validity of our assumptions. The boundary layer along a flat plate is computed; the outer edge boundary conditions are as follows: $p_e = 12525\, Pa$, $T_e = 6000\, K$, $M_e = 0.1,\ 0.3,\ 0.9,\ 2$. The outer edge chemical composition

is considered to be the equilibrium one. The wall is assumed to be at radiative equilibrium and the wall emissivity coefficient is set to 0.85. The reacting mixture is five species air, the wall catalytic reactions are $N + N \rightarrow N_2$ and $O + O \rightarrow O_2$ and the computations are made for two levels of catalytic recombination probability, $\gamma = 0$ and $\gamma = 1$.

In Figs. 12 and 13 the wall heat flux for noncatalytic and fully catalytic wall respectively is shown for all Mach numbers. The heat flux is expressed in function of the normalized coordinate $x(u_{e,M_e=0.1}/u_e)$ that should be the same for all Mach numbers because of Eq. 18.

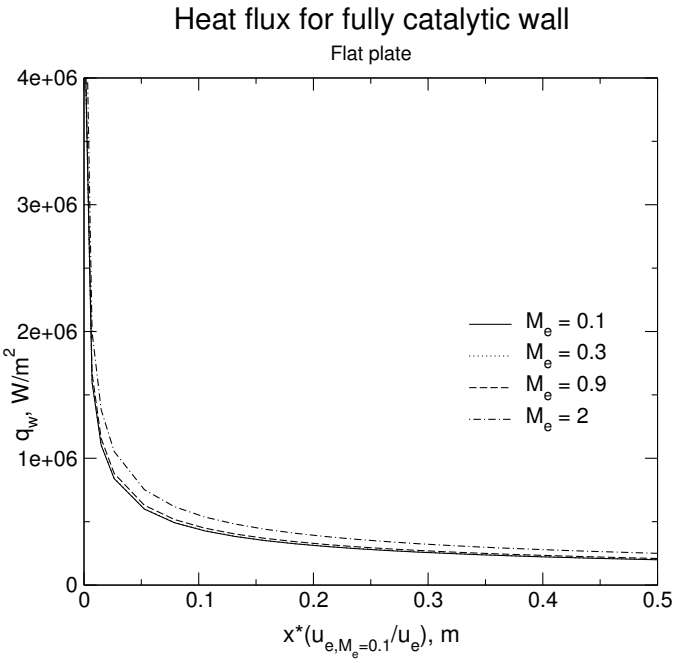

Figure 13: Flat plate heat flux for fully catalytic wall

Supposing we want to simulate the real flight flow with a Mach 0.1 wind tunnel flow, the agreement in heat flux (except for a small region near the flat plate tip, where the classical boundary layer theory is not adequate) ranges from excellent for $M_e = 0.1,\ 0.3,\ 0.9$ to acceptable for $M_e = 2$. The maximum heat flux difference is as follows: for a noncatalytic wall it is around $21\,\%$ between $M_e = 0.1$ and $M_e = 2$, for a fully catalytic wall it is around $18 - 19\,\%$ for the same Mach number range. The heat flux difference is easily explained: it is due to the viscous dissipation that naturally increases with Mach number.

Although the outer edge Mach number is different, the structure of the boundary layer is similar for equal values of the normalized coordinate $x(u_{e,M_e=0.1}/u_e)$ for all cases. Temperature profile and atomic oxygen and atomic nitrogen profiles for noncatalytic wall are shown at the station $x(u_{e,M_e=0.1}/u_e) = 0.5\,m$ in Figs. 14 and 15 respectively. Only the profiles for $M_e = 0.1$ and $M_e = 2$ are shown, the ones for the remaining Mach numbers fall in between the two. The temperature profile agreement is good; the temperature for $M_e = 2$ is slightly higher and has a stronger slope at the wall, as it should be because of the heat generated by viscous dissipation inside the boundary layer. Atomic oxygen and atomic nitrogen profiles match quite well because the first Damköhler number at every x/u_e station is the same for all boundary layers. We also notice that the boundary layer thickness is equal and this is important because, as already discussed in Sec. 5, it ensures that the second Damköhler number is the same and therefore the heterogeneous chemistry-diffusion coupling is well reproduced.

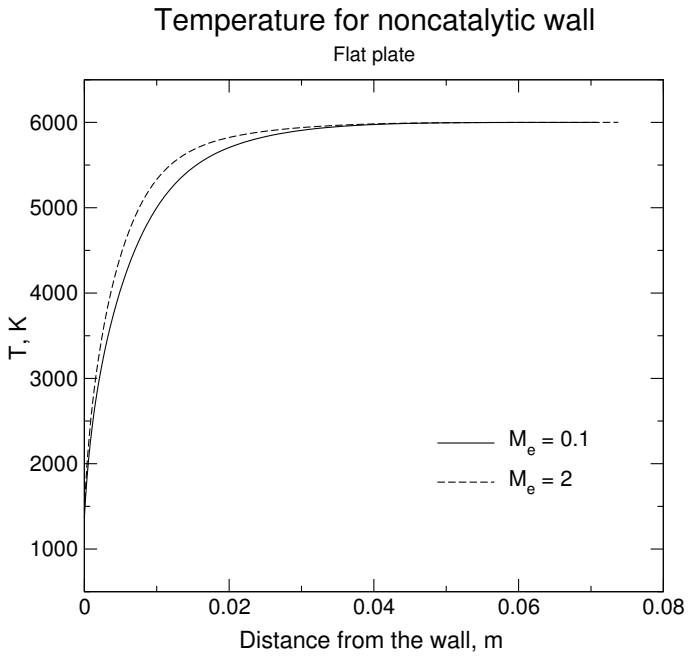

Figure 14: Flat plate temperature at $x(u_{e,M_e=0.1}/u_e) = 0.5$ for noncatalytic wall

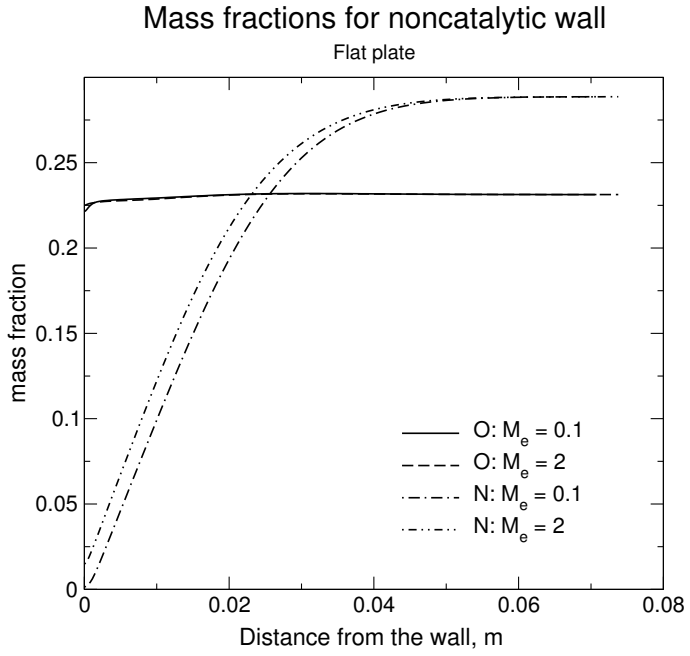

Figure 15: Flat plate O and N mass fraction at $x(u_{e,M_e=0.1}/u_e) = 0.5$ for noncatalytic wall

7 Conclusions

The Local Heat Transfer Simulation concept for stagnation point configurations has been presented with its application to plasma wind tunnel experiments. Two examples allowed to illustrate the different aspects of the methodology and demonstrated that it correctly extrapolates ground test conditions to real flight ones. The equality of stagnation enthalpy, pressure and velocity gradient, plus the fact that the flow is near equilibrium in the stagnation region, are necessary for a correct reproduction of the flight thermochemical environment

inside the ground facility. Deviations from the condition of local equilibrium in the stagnation region of the real body are mainly responsible for the discrepancies in heat flux determination between the ground facility and the flight. However, a normalized heat flux formulation can be used to account for these inconsistencies and to obtain an improved heat flux prediction.

We have also shown a preliminary version of an approximate Local Heat Transfer concept for a flat plate configuration. The heat flux is not duplicated as accurately as in the stagnation point configuration, however first and second Damköhler numbers are well duplicated and therefore also the chemical composition in the boundary layer and the wall heterogeneous chemical reactions phenomena.

References

[1] ANDERSON, J. D. *Hypersonic and High Temperature Gas Dynamics*. McGraw-Hill, New York, 1989.

[2] BARBANTE, P. F. *Accurate and Efficient Modeling of High Temperature Nonequilibrium Air Flows*. PhD thesis, Université Libre de Bruxelles-von Karman Institute, Bruxelles, Belgium, 2001.

[3] BARBANTE, P. F., AND DEGREZ, G. An Efficient Euler/Navier-Stokes Solver for Reacting Flows. In 16^{th} *IMACS World Congress 2000* (21-25 August 2000).

[4] BARBANTE, P. F., DEGREZ, G., AND SARMA, G. S. R. Computation of Nonequilibirum High-Temperature Axisymmetric Boundary-Layer Flows. *Journal of Thermophysics and Heat Transfer 16*, 4 (2002), 490–497.

[5] BOTTIN, B., CHAZOT, O., CARBONARO, M., VAN DER HAEGEN, V., AND PARIS, S. The VKI Plasmatron Characteristics and Performance. In *Measurement Techniques for High Temperature and Plasma Flows*, J. M. Charbonnier and G. S. R. Sarma, Eds. NATO-RTO, 1999.

[6] BOTTIN, B., VANDEN ABEELE, D., CARBONARO, M., DEGREZ, G., AND SARMA, G. S. R. Thermodynamic and Transport Properties for Inductive Plasma Modeling. *Journal of Thermophysics and Heat Transfer 13*, 3 (1999), 343–350.

[7] CHAZOT, O., PARIS, S., COLLIN, P., BICKEL, M., AND ULLMAN, T. Tps Testing and Catalycity Determination in the vki Plasmatron Facility. In 3^{rd} *Atmospheric Reentry Vehicles and System Symposium* (24-27 March 2003).

[8] COQUEL, F., AND LIOU, M. S. Hybrid Upwind Splitting Scheme by a Field by Field Decomposition. TM 106843, NASA, Jan. 1995.

[9] DE LA LLAVE PLATA, M. Analysis and Application of a Methodology for the Determination of TPS Materials Catalycity. Diploma Project Report 2000-4, von Karman Institute, June 2000.

[10] DEGREZ, G., BARBANTE, P. F., DE LA LLAVE PLATA, M., MAGIN, T., AND CHAZOT, O. Determination of the Catalytic Properties of TPS Materials in the VKI ICP Facilities. In *ECCOMAS Computational Fluid Dynamics Conference. Swansea UK* (September 2001).

[11] FAY, J. A., AND RIDDELL, F. R. Theory of Stagnation Point Heat Transfer in Dissociating Air. *Journal of the Aeronautical Sciences 25*, 2 (1958), 73–85.

[12] FLETCHER, C. A. J. *Computational Techniques for Fluid Dynamics*, 2nd ed., vol. 2. Springer-Verlag, Heidelberg, 1991, ch. 15.

[13] GOULARD, R. On Catalytic Recombination Rates in Hypersonic Stagnation Heat Transfer. *Jet Propulsion 28* (1958), 737–745.

[14] GUPTA, R. N., YOS, J. M., THOMPSON, R. A., AND LEE, K. P. A Review of Reaction Rates and Thermodynamic and Transport Properties for an 11-Species Air Model for Chemical and Thermal Nonequilibrium Calculations to 30000 K. RP 1232, NASA, Aug. 1990.

[15] HIRSCH, C. *Numerical Computation of Internal and External Flows*, vol. 2. John Wiley & Sons, Chichester UK, 1990.

[16] KOLESNIKOV, A. F. Combined Measurements and Computations of High Enthalpy and Plasma Flows for Determination of TPM Surface Catalycity. In *Measurement Techniques for High Temperature and Plasma Flows*, J. M. Charbonnier and G. S. R. Sarma, Eds. NATO-RTO, 1999.

[17] KOLODZIEJ, P. Strategy and Approach to tps Design. In *Critical Technologies for Hypersonic Vehicle Development*, D. Gaitonde and D. Fletcher, Eds. NATO-RTO, 2004.

[18] LUNEV, V. V. *Hypersonic Aerodynamics*. Maschinostroenie, Moscow, 1975. (in Russian).

[19] NEUMANN, R. Experimental Methods for Hypersonics: Capabilities and Limitations. In *The second joint Europe/US Short Course in Hypersonics* (Jan. 1989), US Air Force Academy Colorado Springs, CO 80840.

[20] PRABHU, D. System Design Constraints - Trajectory Aerothermal Environments. In *Critical Technologies for Hypersonic Vehicle Development*, D. Gaitonde and D. Fletcher, Eds. NATO-RTO, 2004.

[21] ROSE, P., AND STARK, W. Stagnation Point Heat Transfer Measurements in Dissociating Air. *Journal of the Aeronautical Sciences 25*, 2 (1958), 86–97.

[22] STEWART, D., CHEN, Y., BAMFORD, D., AND ROMANOVSKY, A. Predicting Material Surface Catalytic Efficiency Using Arc-jet Tests. AIAA Paper 95-2013.

[23] SUTTON, K., AND GNOFFO, P. Multi-component Diffusion with Application to Computational Aerothermodynamics. In 7^{th} *AIAA/ASME Joint Thermophysics and Heat Transfer Conference* (15-18 June 1998), AIAA Paper 98-2575.

[24] WHITE, F. M. *Viscous Fluid Flows*, 2nd ed. McGraw-Hill, New York, 1991, ch. 3.

Appendix 1

Nomenclature

$\mathcal{D}_{ij}$	=	binary diffusion coefficient between species i and j, m^2/s
F	=	u/u_e, nondimensional tangential velocity
g	=	h/h_e, nondimensional mixture enthalpy
h	=	mixture static enthalpy, J/kg
H	=	mixture total enthalpy, J/kg
H^{ad}	=	mixture recovery enthalpy, J/kg
h_i	=	enthalpy of species i, J/kg
Le	=	Lewis number
J_i	=	nondimensional mass diffusion flux of species i
l_0	=	$\rho\mu/\rho_e\mu_e$, Chapman-Rubesin parameter
Ns	=	number of species in the mixture
p	=	pressure, Pa
Pr	=	Prandtl number
q	=	heat flux, W/m^2
Q	=	normalized heat flux
R	=	body nose radius, m
T	=	mixture temperature, K
u, v	=	tangential and normal velocity components, m/s
V	=	velocity, m/s
$\tilde{V}$	=	nondimensional transformed normal velocity
$\dot{w}_i$	=	nondimensional mass production rate of species i
x, y	=	Cartesian coordinates, m
y_i	=	mass fraction of species i
β	=	$\partial u/\partial x$, velocity gradient, s^{-1}
γ	=	wall catalytic recombination probability
$\hat{\eta}$	=	transformed y coordinate
λ	=	mixture thermal conductivity, W/(m K)
μ	=	mixture viscosity, m^2/s
ρ	=	mixture density, kg/m^3

Subscripts

w	=	wall surface
e	=	boundary layer outer edge
∞	=	free stream

Superscripts

f	=	flight
FC	=	fully catalytic
NC	=	noncatalytic
t	=	ground facility